Journal of Electroanalytical Chemistry 961 (2024) 118191

Contents lists available at ScienceDirect

Journal of Electroanalytical Chemistry

journal homepage: www.elsevier.com/locate/jelechem

Eco-friendly high entropy oxide rock-salt type structure for oxygen evolution reaction obtained by green synthesis

Jakeline R.D. Santos [a,b,*], Rafael A. Raimundo [c], João F.G. de A. Oliveira [d], Johnnys da S. Hortencio [e], Francisco J.A. Loureiro [f,g], Daniel A. Macedo [h], Marco A. Morales [c], Isacco Gualandi [b], Domenica Tonelli [b,*], Uílame U. Gomes [a,c]

[a] Materials Science and Engineering Postgraduate Program, UFRN, Natal 59078-970, Brazil
[b] Department of Industrial Chemistry "Toso Montanari", Industrial Chemistry, UNIBO, V.le Risorgimento 4, 40136 Bologna, Italy
[c] Department of Theoretical and Experimental Physics, Federal University of Rio Grande do Norte, UFRN, 59078-970 Natal, Brazil
[d] Gleb Wataghin Institute of Physics – R. Sérgio Buarque de Holanda, 777 – Cidade Universitária, 13083-859 Campinas, Brazil
[e] Department of Chemistry, Federal University of Paraíba, UFPB, 58.051-900 João Pessoa, Brazil
[f] TEMA - Centre for Mechanical Technology and Automation, Mechanical Engineering Department, University of Aveiro, 3810-193, Portugal
[g] LASI - Intelligent Systems Associate Laboratory, 4800-058 Guimarães, Portugal
[h] Materials Science and Engineering Postgraduate Program, Federal University of Paraíba, UFPB, 58051-900 João Pessoa, Brazil

ARTICLE INFO

Keywords:
Green synthesis
High entropy oxide
Nanoparticles
Electrocatalysts
Oxygen Evolution Reaction

ABSTRACT

Global energy consumption increases year after year, causing the depletion of non-renewable sources. According to the International Energy Agency (IEA), global demand for electrical energy is expected to increase by 3.3 % in 2024. Therefore, developing new renewable sources is urgent, including new devices for energy storage and conversion, particularly those based on electrochemical reactions. Water splitting is a clean and sustainable technology capable of facing this issue by producing oxygen and hydrogen from water and electricity. However, an issue related to this technology is the slow kinetics of oxygen evolution reaction, making it necessary to develop new electrocatalysts with high electrochemical performance. To meet this requirement, this work deals, for the first time, with a high entropy oxide with a rock-salt structure synthesized by a green sol–gel synthesis using *red seaweed (Rhodophyta)* as a polymerizing agent. Sol-gel synthesis allows the large-scale production of nanomaterials with high uniformity and dispersion of the involved chemical elements. The literature, which discussed the synthesis of these oxides, reveals that agents harmful to the environment are employed, including sodium hydroxide, acetic acid, hexadecyltrimethylammonium bromide, urea, and ammonium hydroxide. The composition of the high entropy oxide is $(Mg_{0.2}Ni_{0.2}Co_{0.2}Cu_{0.2}Zn_{0.2})O$. As electrocatalyst for oxygen evolution reaction, it exhibits a low overpotential (336 mV *vs.* RHE at 10 mA cm^{-2}), a Tafel slope of 68 mV dec^{-1}, and excellent durability. The electrochemical performance of the high entropy oxide prepared in this work is superior to other electrocatalysts of the same class that were produced using transition metal-based precursors.

1. Introduction

In recent decades, mainly due to the advent of new technologies with the exponential growth of the population, there has been a search for the development of new materials with better functional properties [1]. In this scenario, the class of high entropy ceramic materials stands out among various groups, such as carbides, borides, nitrides, and oxides [2]. High entropy oxides (HEO) [3] or entropy stabilized oxides (ESO) have attracted much attention due to their remarkable physicochemical properties such as thermal and chemical stability, enormous dielectric constant, electrocatalytic performance, stability, increased ionic conductivity, magnetic properties, besides being environmentally friendly and low cost [4–9]. Furthermore, HEO are solid solutions of MO_6 species formed by five or more different cations (M) with equimolar or nearly equimolar concentrations, which generate synergistic effects producing thermodynamic stabilizations to obtain a highly configurable system entropy [7,8].

Based on the above concept, the first high entropy oxide

* Corresponding authors at: Department of Industrial Chemistry "Toso Montanari", Industrial Chemistry, UNIBO, V.le Risorgimento 4, 40136 Bologna, Italy.
E-mail addresses: jakeline.dorados@unibo.it (J.R.D. Santos), domenica.tonelli@unibo.it (D. Tonelli).

https://doi.org/10.1016/j.jelechem.2024.118191
Received 9 January 2024; Received in revised form 28 February 2024; Accepted 12 March 2024
Available online 22 March 2024

$Ni_xMg_xCo_xCu_xZn_xO$ system with (x = 0.2) was synthesized in 2015 by Rost et al. [8]. Later, in 2017, they used the EXAFS technique to observe and understand the average local environment surrounding individual absorbing species [10]. The samples were prepared by the solid state reaction method from a mixture of the divalent oxides of NiO, MgO, CoO, CuO and ZnO. They were able to obtain a single-phase, characterized by the rock-salt crystal structure (face-centered cubic-FCC), despite the different crystalline structure usually found for Cu oxides (tenorite, monoclinic) and Zn (wurzite, hexagonal) with space group (*C*2/*c*) and (*P*63*mc*), respectively [11]. The high entropy oxides can be synthesized by other methods such as combustion [12], citrate precursor [2], co-precipitation [13], spray pyrolysis [14], solvo/hydrothermal [15], and sol–gel [16].

Among them, the proteic sol–gel method is based on the green synthesis and provides a solution to the negative effects of chemical and physical methods, such as toxicity, due to the harmful substances which are released in the environment [17]. Moreover, it is considered a versatile, fast, easy-to-perform, and low-cost [18,19]. The method uses a gelatin (Agar-agar) obtained from a red algae of the type *Rhodophyta*, which has the function of polymerizing agent to synthesize complex oxides [20,21]. Other polymerizing agents can be, for example, commercial gelatin [22], and coconut water [23].

Agar-agar is a polysaccharide extracted from two different species of red seaweed (*Gracilaria* sp. and *Gelidium* sp.), and forms the supporting structure in the cell walls of those vegetables [24]. In addition, it is a biopolymer, hydrocolloid, and a polysaccharide source which, when in contact with water, forms a gel, called mucilage. Agar-agar is constituted by a heterogeneous mixture of two types of polysaccharides: agarose, a neutral polymer, and agaropectin, a charged sulfated polymer. Agarose is the molecule responsible for the gelling action of agar-agar [25]. Due to its gelling properties, non-toxicity, biodegradability, and biocompatibility [24], it is widely used in food, cosmetics, and pharmaceutical industries, among others [25].

High entropy oxides can be used in various technological applications, such as catalysis, lithium-ion batteries, electrocatalysis, and energy storage and conversion devices [15,26,27]. Regarding the energy conversion processes, the electrochemical water splitting takes place through two semi-reactions: Hydrogen Evolution Reaction (HER) and Oxygen Evolution Reaction (OER) [15,28]. For the OER occurrence, a high overpotential is required to transfer the four electrons involved in the reaction, leading to a slow kinetics and low efficiency of the process [29]. Therefore, it is important to develop new electrocatalysts in order to reduce the overpotential and accelerate the reaction [30]. It is well known that the most efficient electrocatalysts are iridium and ruthenium oxides, but their high cost and scarcity in nature have limited their large-scale applications [15]. Therefore, one of the main challenges in electrocatalysis is the development of materials with high electrochemical performance, low cost and composed of elements that are earth-abundant [7,15,26]. An example is the chemical compound used in this work which, in addition to having the characteristics mentioned above, displays a phase stabilization effect driven by entropy, mainly due to the high-temperature stability of Co, Ni and Cu [31,32]. Within this perspective, a catalyst made of high entropy oxides emerge as an alternative for OER processes.

The main purpose of the present work is to synthesize a high entropy oxide of the type $(Mg_{0.2}Ni_{0.2}Co_{0.2}Cu_{0.2}Zn_{0.2})O$ by the green synthesis method using agar-agar as a polymerizing agent and to study its structural, morphological, optical and electrochemical properties.

2. Materials and methods

2.1. Chemicals

All the reagents were of analytical grade and used without further purification. Magnesium nitrate ($Mg(NO_3)_2{\cdot}6H_2O$), nickel nitrate ($Ni(NO_3)_2{\cdot}6H_2O$), cobalt nitrate ($Co(NO_3)_2{\cdot}6H_2O$), copper nitrate ($Cu(NO_3)_2{\cdot}3H_2O$), zinc nitrate ($Zn(NO_3)_2{\cdot}6H_2O$) and Nafion solution (5 wt %) were acquired from Sigma-Aldrich (Saint-Louis, MO, USA). Isopropyl alcohol was obtained from Synth. Agar-agar was purchased from Gelialgas-Argargel (João Pessoa, Brazil). Nickel foam (porosity > 95 %) was purchased from QiJing Ltd., Ninghai, China. The electrode made with Ni foam has a square like shape with size of 1 cm^2.

2.2. Green synthesis

The green synthesis method was used to obtain the high entropy oxide $Mg_xNi_xCo_xCu_xZn_xO$ (x = 0.2) using agar-agar as the polymerizing agent. The amounts of the Mg, Ni, Co, Cu, and Zn nitrates were equimolar, each equal to 5.7 mmol (totalizing 28.5 mmol).

The synthesis was performed in several steps. First, the polymer solution was prepared by mixing 2.0 g of agar-agar and 50 mL of distilled water at 60 °C, under stirring. Then, after adding the metal salts, the resulting solution was warmed up to 90 °C and kept under stirring until a gel was formed. Afterwards, the gel was pre-calcined at 350 °C for 2 h, the obtained powder was grinded and calcined at 900 °C for 2 h. Finally, the pre-calcination and calcination steps were repeated. All steps to obtain the high entropy oxide and the microstructural and electrochemical characterizations are shown in Fig. 1.

2.3. Characterizations

2.3.1. Structural and morphological characterization

The crystalline properties of the high entropy oxide were studied by X-ray diffractometry (XRD) by employing a Shimadzu XRD-7000 diffractometer, endowed with a Cu Kα source with wavelength λ = 1.5418 Å. The morphology and chemical homogeneity of the sample were investigated by field emission scanning electron microscopy (FESEM, Carl Zeiss, Supra 35-VP Model) equipped with a Bruker EDS detector (XFlash 410-M). Fourier transform infrared spectroscopy (FTIR) spectra of powders were obtained using a Shimadzu IRTracer-100 spectrometer, between 400 and 4000 cm^{-1}, using KBr pellets. Raman spectroscopy measurements were performed at room temperature using a laser with 532 nm as the excitation source. Magnetic measurements were obtained using a vibrating sample magnetometer (VSM) from Lakeshore, model 7400, at room temperature, with an applied maximum magnetic field of +15.0 kOe. The chemical states of the elements at the surface of the nanoparticles were studied by X-ray Photoelectron Spectroscopy (XPS) using a SPECS Phoibos 150 spectrometer with a monochromatized Al Kα X-ray source (1486.6 eV).

2.3.2. Electrochemical characterization

With regard to the electrochemical measurements, cyclic voltammetry (CV), linear sweep voltammetry (LSV), electrochemical impedance spectroscopy (EIS), and chronopotentiometry were carried out using a PGSTAT204 potentiostat/galvanostat with a FRA32M (Metrohm Autolab) and a conventional three-electrode cell, consisting of the Ag/AgCl reference electrode, a platinum wire as the counter electrode, and the sample of the high entropy oxide deposited on Ni foam used as working electrode, in a 1 M KOH electrolyte solution. The catalytic ink was prepared by mixing 5 mg of the HEO sample with 500 μL of isopropyl alcohol and dispersing the mixture in 50 μL of Nafion solution. Then, the ink was drop-casted onto clean substrates of Ni foam and dried at room temperature for 24 h. The potential was converted from Ag/AgCl to the reversible hydrogen electrode (RHE) according to the following Eq. (1):

$$E_{RHE} = E_{vsAg/AgCl} + E^0_{(Ag/AgCl)} + 0.0059\,pH \quad (1)$$

LSV measurements (sweep rate of 5 mV s^{-1}) were performed from 0 to 1 V *vs*. Ag/AgCl with iR correction. The overpotential (η_{10}) was calculated at a current density of 10 mA cm^{-2}, according to the Eq. (2):

$$\eta_{10} = E_{RHE} - 1.23\ V \quad (2)$$

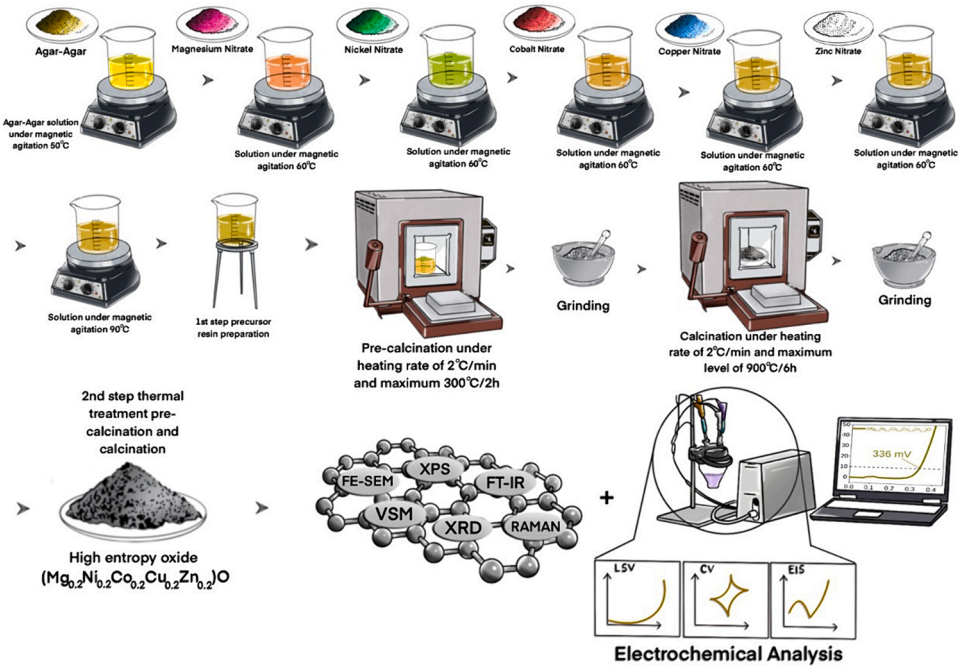

Fig. 1. Steps involved in the green synthesis process of high entropy oxide $(Mg_{0.2}Ni_{0.2}Co_{0.2}Cu_{0.2}Zn_{0.2})O$, and microstructural and electrochemical characterizations carried out.

Chronopotentiometry measurements were performed at a fixed current density of 10 mA cm^{-2} for a time interval of 10 h. Impedance experiments were performed at the potential values of 0.5, 0.6, and 0.65 V (*vs.* RHE) from 0.1 to 10 kHz and a voltage amplitude of 10 mV. CV scan rates were varied between 5 mV s^{-1} and 200 mV s^{-1}. The electrical double layer capacitance (C_{DL}) of the electrode was measured in a non-Faradaic region, determined from the LSV, recording CVs at various scan rates. Depending on the electrical system, the specific capacitance for materials based on transition metals is (C_s, 40 μF cm^{-2}) [33] was used in the calculation of the electrochemically active surface area (ECSA) by the following Eq. (3):

$$ECSA = C_{DL}/C_s \quad (3)$$

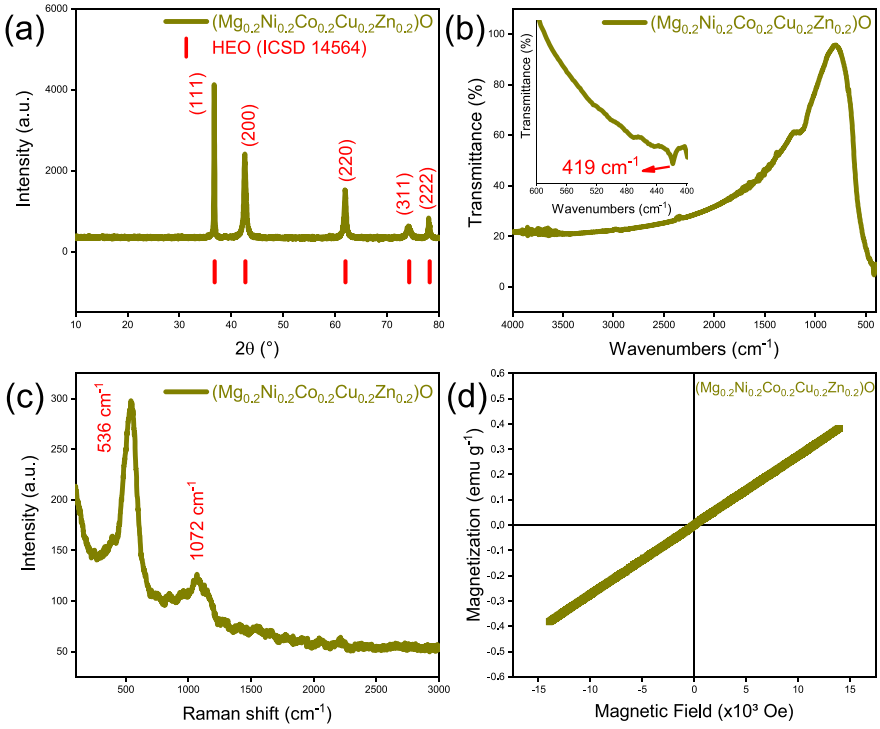

Fig. 2. (a) X-ray diffraction, (b) Fourier transform infrared spectroscopy, (c) Raman spectrum and (d) vibrating-sample magnetometry of $(Mg_{0.2}Ni_{0.2}Co_{0.2}Cu_{0.2}Zn_{0.2})O$.

3. Results and discussion

3.1. Microstructural characterization

Fig. 2 shows the structural and magnetic characteristics of $(Mg_{0.2}Ni_{0.2}Co_{0.2}Cu_{0.2}Zn_{0.2})O$. As seen in Fig. 2a, all observed reflections are well-defined and characteristic of a solid solution with rock-salt structure (with lattice parameters a = b = c = 4.235 Å, ICSD no. 14564, space group *Fm*-3*m* (225)) [34]. Five diffraction peaks located at 36.7°, 42.62°, 61.92°, 74.14°, and 78.04° are indexed to the crystal planes (111), (200), (220), (311) and (222), respectively. Within the XRD sensitivity no other oxide phases were detected, although existing literature on high entropy oxides has revealed that copper oxide phases can precipitate during the cooling stage, hindering the formation of a single-phase compound [35,36]. This precipitation occurs when the sample is slowly cooled after the sintering treatment. For instance Nallathambi et al. [35] noticed the formation of a CuO second phase in their HEO when the samples were cooled at rates equal or smaller than 5 °C min^{-1}. In our work, there was no precipitation, as the sample was air quenched immediately after the sintering. The FTIR spectrum of $(Mg_{0.2}Ni_{0.2}Co_{0.2}Cu_{0.2}Zn_{0.2})O$ is shown in Fig. 2b. According to Usharani et al. [34] and Su et al. [37], the band located below 500 cm^{-1} (insert in Fig. 2b) is attributed to the presence of cations in the lattice, and indicates the formation of a metal–oxygen bond. Raman spectroscopy was performed from 150 to 3000 cm^{-1} to investigate the structure of the high entropy oxide, and the relevant spectrum is shown in Fig. 2c. The bands located at 536 cm^{-1} and 1072 cm^{-1} are the result of the 1P LO and 2P LO modes, which indicate the formation of an asymmetric structure [37] and the Frohlich interaction between the second-order longitudinal optical phonon and the local free carrier [38]. The magnetization (M) versus magnetic field (H) measurement was obtained to study the magnetic state of the sample at room temperature. Since Cu^{2+} has one unpaired electron in the d-orbital, this ion is magnetic. Co^{2+} and Ni^{2+} in their high spin states have three and two unpaired electrons in their d-orbitals, respectively, so these ions are magnetic too. As Co, Ni, and Cu represent 60 % of the total amount of cations in the lattice, a magnetic ordered structure is expected. As observed in Fig. 2d, the M-H curve shows a linear behaviour with a positive angular coefficient. This result suggests that the sample could be antiferromagnetic at room temperature. In fact, Usharani et al. studied $(Mg_{0.2}Ni_{0.2}Co_{0.2}Cu_{0.2}Zn_{0.2})O$, by performing magnetization versus temperature (5–300 K) measurements, and concluded that their sample was antiferromagnetic in the whole range of temperatures [39]. That confirms that green synthesis using agar-agar as polymerizing agent is efficient in producing high entropy oxides. The effectiveness of agar-agar has also been proven for the syntheses of simple oxides [40], ferrites [35], and cobaltites [21,42].

FESEM analyses accompanied by chemical mapping and energy dispersive X-ray spectroscopy of $(Mg_{0.2}Ni_{0.2}Co_{0.2}Cu_{0.2}Zn_{0.2})O$ are shown in Fig. 3. As seen in Fig. 3a–b, the FESEM images reveal the formation of spherical aggregated grains, with particle sizes larger than 1 μm, characteristic of samples obtained at high calcination temperatures (900 °C). The mapping (Fig. 3c) shows the elements Mg (green, Fig. 3c1), Ni (indigo blue, Fig. 3c2), Co (purple, Fig. 3c3), Cu (red, Fig. 3c4), Zn (yellow, Fig. 3c5) and O (blue, Fig. 3c6) uniformly distributed throughout all micrometric particles and without visible segregations, thus confirming the chemical and microstructural homogeneity. The spectrum of $(Mg_{0.2}Ni_{0.2}Co_{0.2}Cu_{0.2}Zn_{0.2})O$ is shown in Fig. 3d. The spectral atomic percentages of Mg, Ni, Co, Cu and Zn resulted 18.11, 19.55, 21.08, 21.14, and 20.12, respectively. The result reveals that the composition obtained experimentally is in agreement with the nominal composition.

To understand the surface chemical composition of the $(Mg_{0.2}Ni_{0.2}Co_{0.2}Cu_{0.2}Zn_{0.2})O$ sample, X-ray photoelectron spectroscopy (XPS) was performed, and the spectra are displayed in Fig. 4. The Mg $2p_{3/2}$ core level is shown in Fig. 4a, displaying one main peak related to MgO [43]. Fig. 4b shows the high-resolution Ni $2p_{3/2}$ spectrum, which was fitted to three contributions. The peak at the lowest binding energy (855.170 eV) is close to that reported for NiO, the other two peaks are related to shake-up satellite features [44]. Conversely, the high-resolution spectra obtained for the Co $2p_{3/2}$ and the Cu $2p_{3/2}$ core levels were each deconvoluted into two main peaks (Fig. 4c and 4d, respectively). In both cases, the first peak at lower binding energy corresponds to CoO [45] or CuO [46,47], whereas the second peak can be ascribed to $Co(OH)_2$ [45] or $Cu(OH)_2$ [47]. In addition, at higher binding energies, two additional peaks were further deconvoluted for both Cu $2p_{3/2}$ and the Co $2p_{3/2}$ core levels, corresponding to the shake-up satellite features [45,47]. The Zn $2p_{3/2}$ core level is shown in Fig. 4e, displaying one main peak related to

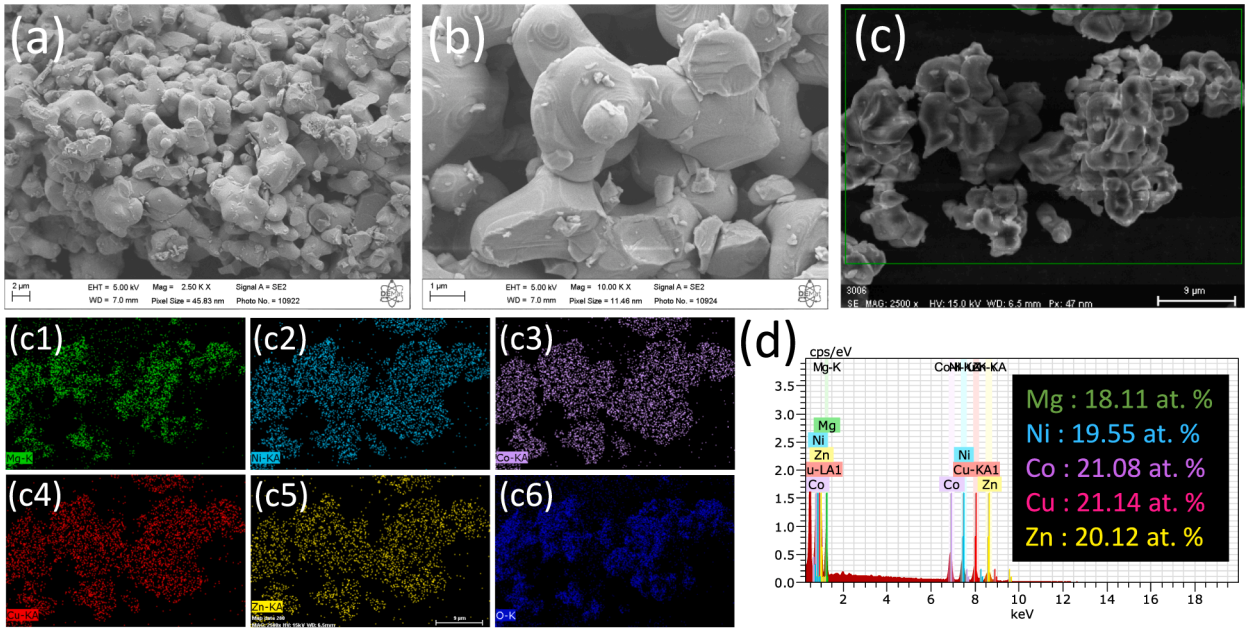

Fig. 3. (a-c) Scanning electron microscopy images at different magnifications, (c1-c6) Elemental mapping images and (d) typical EDS spectra of $(Mg_{0.2}Ni_{0.2}Co_{0.2}Cu_{0.2}Zn_{0.2})O$.

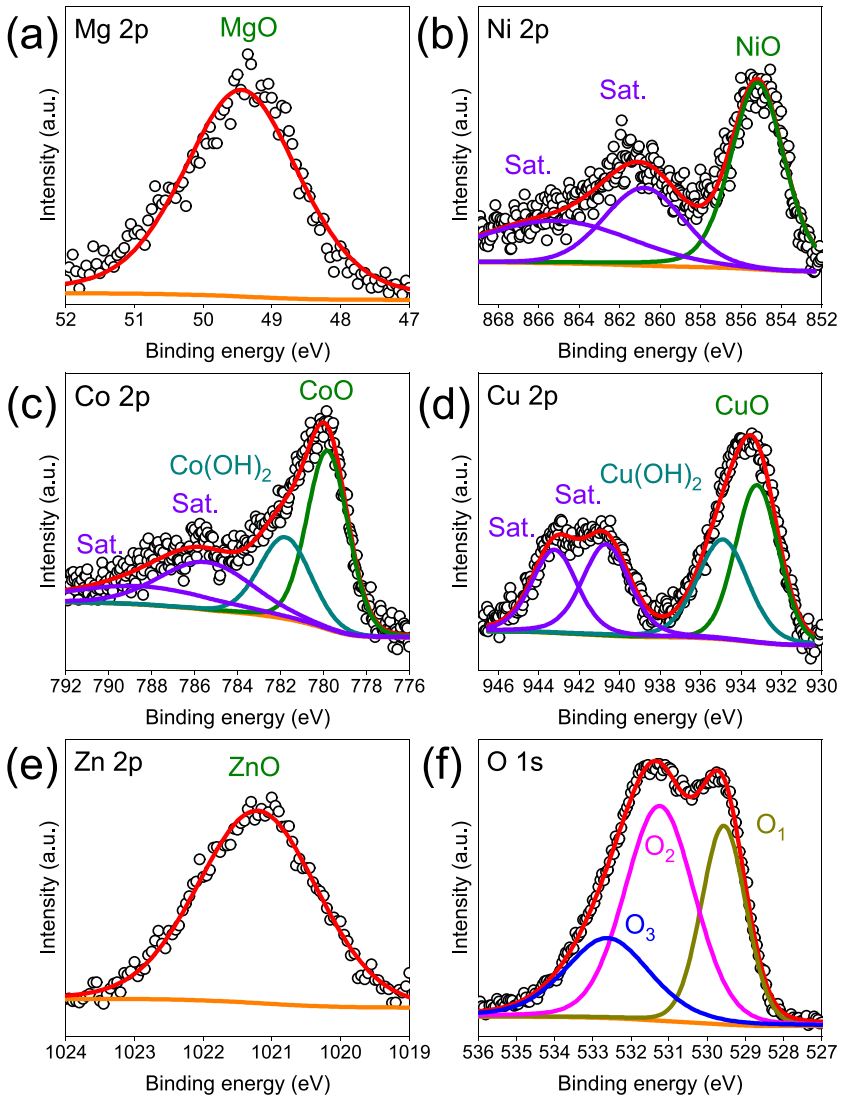

Fig. 4. X-ray photoelectron spectroscopy (XPS) spectra of $(Mg_{0.2}Ni_{0.2}Co_{0.2}Cu_{0.2}Zn_{0.2})O$ obtained at high-resolution (a) Mg 2p, (b) Ni 2p, (c) Co 2p, (d) Cu 2p, (e) Zn 2p, and (f) O 1s regions.

ZnO [48]. Finally, the high-resolution O 1s core-level spectrum is depicted in Fig. 4f, showing three main contributions. The first peak, O_1, at approximately 529.569 eV is due to the presence of lattice oxygen at the surface (O_{lat}, O^{2-}), whereas the second peak, O_2, at nearly 531.245 eV is ascribed to surface chemisorbed oxygen species, O_{ads}, O^{2-}, O_2^{2-}, and O^{-}. The third contribution, O_3, at 532.613 eV is related to unavoidable surface physically adsorbed/residual water molecules (O_{H2O}), in accordance with previous works [41,49,50]. Therefore, it is observed from the EDS analyses and XPS, that the elements are homogeneously distributed across the surface, which generates synergistic effects of the different cations, contributing to the high configurational entropy, lattice distortion, formation of a single phase, high density of oxygen vacancies, more active sites and load transfer capacity. These features lead to a better electrocatalytic performance through the intermediate species of the reaction, such as *O, *OH and *O—OH, and longer stability, as verified in the next paragraph [51,52].

3.2. OER performance

The electrochemical performance of the HEO for OER was evaluated by several electrochemical techniques, including LSV, CV, chronopotentiometry, and EIS. The results from LSV and Tafel slope of $(Mg_{0.2}Ni_{0.2}Co_{0.2}Cu_{0.2}Zn_{0.2})O$ were compared with those obtained from Ni foam, which has been widely used as an electrode support material, due to its excellent physical properties, such as three-dimensional structure, high conductivity, high porosity, resistance in alkaline media and low cost for commercialization [53]. According to the polarization curves (Fig. 5a), overpotentials of 336 and 515 mV *vs.* RHE were determined at 10 mA cm^{-2} for $(Mg_{0.2}Ni_{0.2}Co_{0.2}Cu_{0.2}Zn_{0.2})O$ and Ni foam, respectively. The electrochemical performance of $(Mg_{0.2}Ni_{0.2}Co_{0.2}Cu_{0.2}Zn_{0.2})O$ over the entire current density range is presented in Fig. 5b. The overpotential of our sample is compatible with the one displayed by other high entropy oxides prepared by high-energy milling ($((Co_{0.2}Ni_{0.2}Mn_{0.2}Zn_{0.2}Fe_{0.2})_3O_{3.2}$, $\eta = 336$ mV) [54]. Furthermore, our electrocatalyst has greater OER activity than $(Co,Cu,Fe,Mn,Ni)_3O_4$ ($\eta = 400$ mV) [55], $SrNb_{0.1}Co_{0.7}Fe_{0.2}O_{3-\delta}$ ($\eta = 390$ mV) [56], $(Fe_{0.73}Cr_{0.71}Co_{0.78}Ni_{0.81}Al_{0.1})O_{4.01}$ ($\eta = 381$ mV) [51,57]. Generally, the results observed in our research for the high entropy oxide with the rock-salt structure agree well with the results of the best electrocatalysts reported in the literature (Table S1). The overpotential of the HEO investigated in the present work, equal to 336 mV at 10 mA cm^{-2}, is lower than the one displayed by commercial iridium oxide (400 mV, at 10 mA cm^{-2}) [58].

To thoroughly understand the oxygen evolution reaction process, the Tafel slope of the electrocatalyst was obtained from the linear scanning voltammetry, as well as cyclic voltammetry experiments were

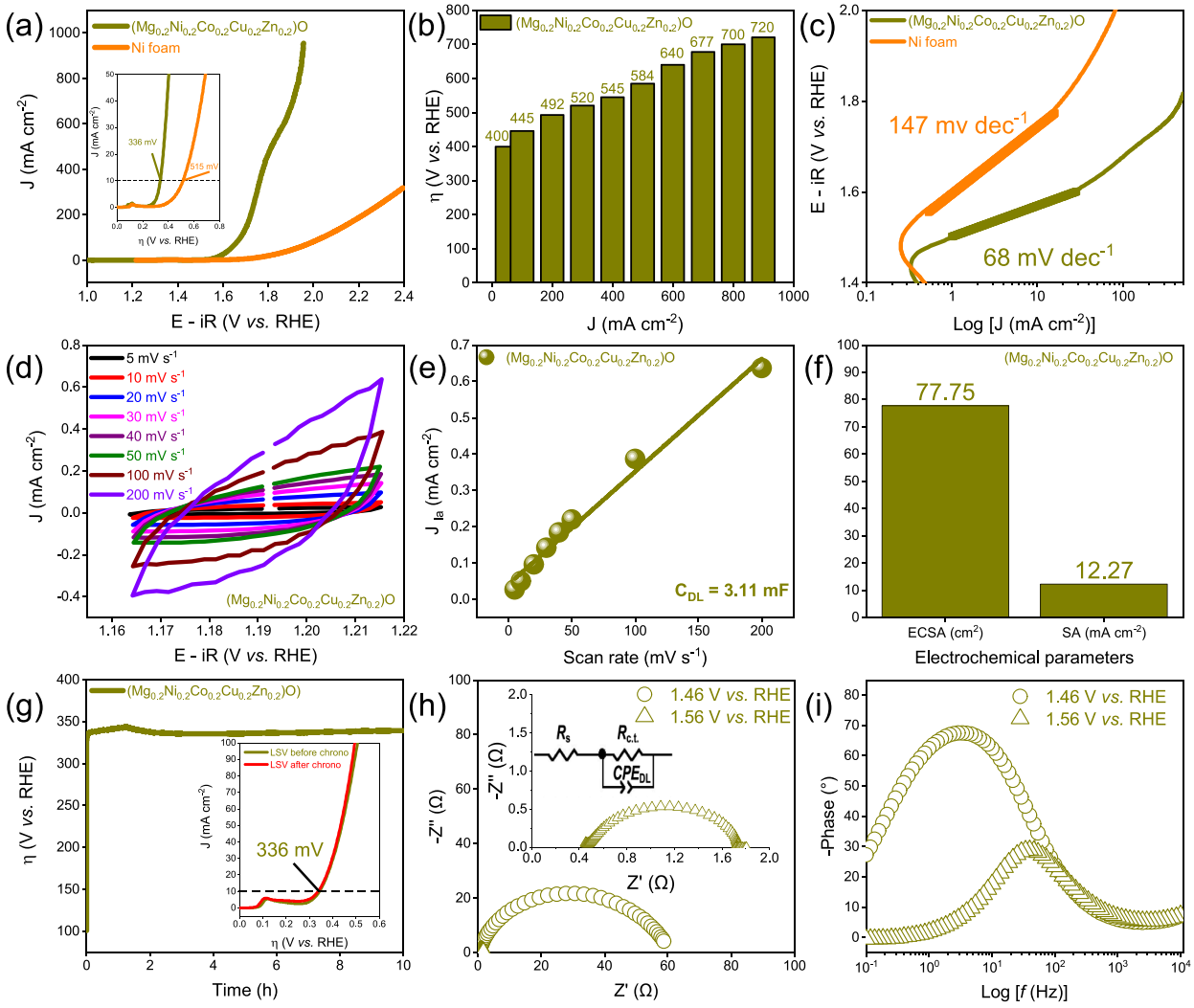

Fig. 5. (a) LSV curves, (b) overpotential at different current densities, (c) Tafel slopes, (d) cyclic voltammetry, (e) electrical double layer capacitance, (f) electrochemical active surface area/specific activity, (g) chronopotentiometry test at J = 10 mA cm^{-2} for 10 h, (h) Nyquist plot accompanied by the equivalent circuit and (i) Bode plot.

conducted to determine the double-layer capacitance (C_{DL}, mF), the electrochemical active surface area (ECSA = C_{DL}/C_s, where C_S = 0.04 mF cm^{-2} was used for materials based on transition metals) [33] and specific activity (SA = J/ECSA, where J represents the density of current at a potential of 1.9559 V *vs.* RHE). Fig. 5c shows the Tafel slopes for $(Mg_{0.2}Ni_{0.2}Co_{0.2}Cu_{0.2}Zn_{0.2})O$ and Ni foam, where it is possible to observe values of 68 mV dec^{-1} and 147 mV dec^{-1}, respectively. These results indicate that $(Mg_{0.2}Ni_{0.2}Co_{0.2}Cu_{0.2}Zn_{0.2})O$ has greater electrocatalytic and kinetic activity for the oxygen evolution reaction. The CVs obtained at various scan rates (5–200 mV s^{-1}) in the potential range of 1.16–1.21 V *vs.* RHE are presented in Fig. 5d. The C_{DL} of $(Mg_{0.2}Ni_{0.2}Co_{0.2}Cu_{0.2}Zn_{0.2})O$ was obtained by linear adjustment of the CV results and was determined to be 3.11 mF (Fig. 5e), thus generating ECSA and SA values of 77.75 cm^2 and 12.27 mA cm^{-2} (Fig. 5f), respectively. The chronopotentiometry test for a time interval of 10 h at 10 mA cm^{-2} was conducted to verify the stability of the electrocatalyst, and its result is presented in Fig. 5g. As observed, the overpotential remains almost constant, demonstrating that $(Mg_{0.2}Ni_{0.2}Co_{0.2}Cu_{0.2}Zn_{0.2})O$ has good electrochemical stability. In addition to this observation, the inset in Fig. 5g shows that LSV traces, before and after chronopotentiometry tests, overlap so proving once again the excellent stability of the catalys.

The electrocatalytic assessment was complemented by electrochemical impedance spectroscopy to assist in understanding the OER kinetics of the $(Mg_{0.2}Ni_{0.2}Co_{0.2}Cu_{0.2}Zn_{0.2})O$ sample. The EIS spectra were recorded at two different DC potentials (1.46 and 1.56 V *vs.* RHE), both in the OER regime. Fig. 5h shows the Nyquist plot consisting of a high-frequency resistance, R_s (uncompensated solution resistance), followed by a large semicircle that can be attributed to the total polarization resistance of the electrode, R_p (and denotes the overall rate of the OER process). The data were fitted using the equivalent circuit shown in Fig. 5h, which contains two resistances (R_s, $R_{c.t.}$) and a constant phase element (CPE_{DL}) parallel to $R_{c.t}$ (the resistance to the charge transfer), aiming to represent the double-layer capacitive phenomenon.

Table S2 lists the electrochemical parameters extracted from the equivalent circuit model analysis of the $(Mg_{0.2}Ni_{0.2}Co_{0.2}Cu_{0.2}Zn_{0.2})O$ sample in the OER regime. R_s was found to be effectively constant at both applied potentials. However, we may observe a drastic decrease in R_p with increasing the applied DC potential, as a result of an increased OER kinetics. This enhanced behavior is also demonstrated in the Bode plot presented in Fig. 5i, which shows the phase angle as a function of the measured frequency, where the dominant peak shows a lower magnitude for increased DC potentials. Interestingly, at the same time, C_{DL} was found to decrease in such conditions (Table S2). This behavior can be attributed to the momentaneous decrease in the surface area of the electrocatalyst due to the presence of gas bubbles formed on its surface, which aggravates at higher potentials [59–61].

4. Conclusions

In this work, we synthesized a high entropy oxide of the type $(Mg_{0.2}Ni_{0.2}Co_{0.2}Cu_{0.2}Zn_{0.2})O$ using a green synthesis method and evaluated the performance for OER in an alkaline environment. The microstructural and magnetic properties of the electrocatalyst were elucidated using XRD, FE-SEM, FT-IR, RAMAN, XPS, and magnetometry techniques. The electrochemical properties were investigated using several techniques. Thus, the $(Mg_{0.2}Ni_{0.2}Co_{0.2}Cu_{0.2}Zn_{0.2})O$ exhibited excellent electrocatalytic activity for OER, with overpotential and Tafel slope of 336 mV *vs.* RHE and 68 mV dec^{-1}, respectively, as well as electrochemical stability, as confirmed by chronopotentiometry measurements. The excellent OER activity is ascribed to the synergistic effect of the transition metals present in the high entropy oxide, as well as to the synthesis method presented here.

CRediT authorship contribution statement

Jakeline R.D. Santos: Conceptualization, Validation, Methodology, Formal analysis, Software, Investigation, Writing – original draft. **Rafael A. Raimundo:** Writing – original draft, Software, Investigation, Data curation. **João F.G. de A. Oliveira:** Software. **Johnnys da S. Hortencio:** Software. **Francisco J.A. Loureiro:** Writing – original draft, Software, Investigation. **Daniel A. Macedo:** Writing – review & editing. **Marco A. Morales:** Writing – review & editing, Software, Data curation. **Isacco Gualandi:** Writing – review & editing. **Domenica Tonelli:** Writing – review & editing. **Uílame U. Gomes:** Writing – review & editing.

Declaration of competing interest

The authors declare the following financial interests/personal relationships which may be considered as potential competing interests: 'Jakeline raiane dora dos santos reports was provided by University of Bologna. Jakeline raiane dora dos santos has patent pending to BR 10 2018 011500 6. If there are other authors, they declare that they have no known competing financial interests or personal relationships that could have appeared to influence the work reported in this paper'.

Acknowledgments

Rafael A. Raimundo and Jakeline R. D. Santos acknowledge the national research Council (CNPq, Processes no. 151879/2022-2 and no. 201055/2022-8). Francisco J. A. Loureiro is thankful for the following grants/projects: https://doi.org/10.54499/2020.02797.CEECIND/CP1589/CT0030, http://doi.org/10.54499/PTDC/CTM-CTM/2156/2020, https://doi.org/10.54499/2022.02498.PTDC, https://doi.org/10.54499/UIDB/00481/2020, and https://doi.org/10.54499/UIDP/00481/2020 from Fundação para a Ciência e a Tecnologia (FCT), and CENTRO-01-0145-FEDER-022083 from Centro Portugal Regional Operational Programme (Centro2020), under the PORTUGAL 2020 Partnership Agreement, through the European Regional Development Fund (ERDF).

Appendix A. Supplementary material

Supplementary material to this article can be found online at https://doi.org/10.1016/j.jelechem.2024.118191.

References

[1] P. Koltun, Materials and sustainable development, Prog. Nat. Sci. Mater. Int. 20 (2010) 16–29, https://doi.org/10.1016/s1002-0071(12)60002-1.
[2] A. Kumar, G. Sharma, A. Aftab, M.I. Ahmad, Flash assisted synthesis and densification of five component high entropy oxide (Mg, Co, Cu, Ni, Zn)O at 350 °C in 3 min, J. Eur. Ceram. Soc. 40 (2020) 3358–3362, https://doi.org/10.1016/j.jeurceramsoc.2020.02.036.
[3] Z. Sun, Y. Zhao, C. Sun, Q. Ni, C. Wang, H. Jin, High entropy spinel-structure oxide for electrochemical application, Chem. Eng. J. 431 (2022) 133448, https://doi.org/10.1016/j.cej.2021.133448.
[4] D. Bérardan, S. Franger, A.K. Meena, N. Dragoe, Room temperature lithium superionic conductivity in high entropy oxides, J. Mater. Chem. A. 4 (2016) 9536–9541, https://doi.org/10.1039/c6ta03249d.
[5] Z. Lei, X. Liu, R. Li, H. Wang, Y. Wu, Z. Lu, Ultrastable metal oxide nanotube arrays achieved by entropy-stabilization engineering, Scr. Mater. 146 (2018) 340–343, https://doi.org/10.1016/j.scriptamat.2017.12.025.
[6] D. Bérardan, S. Franger, D. Dragoe, A.K. Meena, N. Dragoe, Colossal dielectric constant in high entropy oxides, Phys. Status Solidi – Rapid Res. Lett. 10 (2016) 328–333, https://doi.org/10.1002/pssr.201600043.
[7] A. Sarkar, Q. Wang, A. Schiele, M.R. Chellali, S.S. Bhattacharya, D. Wang, T. Brezesinski, H. Hahn, L. Velasco, B. Breitung, High-entropy oxides: fundamental aspects and electrochemical properties, Adv. Mater. 31 (2019), https://doi.org/10.1002/adma.201806236.
[8] C.M. Rost, E. Sachet, T. Borman, A. Moballegh, E.C. Dickey, D. Hou, J.L. Jones, S. Curtarolo, J.P. Maria, Entropy-stabilized oxides, Nat. Commun. 6 (2015), https://doi.org/10.1038/ncomms9485.
[9] C. Oses, C. Toher, S. Curtarolo, High-entropy ceramics, Nat. Rev. Mater. 5 (2020) 295–309, https://doi.org/10.1038/s41578-019-0170-8.
[10] C.M. Rost, Z. Rak, D.W. Brenner, J.P. Maria, Local structure of the MgxNixCoxCuxZnxO(x=0.2) entropy-stabilized oxide: an EXAFS study, J. Am. Ceram. Soc. 100 (2017) 2732–2738, https://doi.org/10.1111/jace.14756.
[11] S.H. Albedwawi, A. AlJaberi, G.N. Haidemenopoulos, K. Polychronopoulou, High entropy oxides-exploring a paradigm of promising catalysts: a review, Mater. Des. 202 (2021) 109534, https://doi.org/10.1016/j.matdes.2021.109534.
[12] A. Gautam, M.I. Ahmad, Low-temperature synthesis of five component single phase high entropy oxide, Ceram. Int. 47 (2021) 22225–22228, https://doi.org/10.1016/j.ceramint.2021.04.128.
[13] M. Biesuz, L. Spiridigliozzi, G. Dell'Agli, M. Bortolotti, V.M. Sglavo, Synthesis and sintering of (Mg, Co, Ni, Cu, Zn)O entropy-stabilized oxides obtained by wet chemical methods, J. Mater. Sci. 53 (2018) 8074–8085, https://doi.org/10.1007/s10853-018-2168-9.
[14] B. Cheng, H. Lou, A. Sarkar, Z. Zeng, F. Zhang, X. Chen, L. Tan, K. Glazyrin, H.-P. liermann, J. Yan, L. Wang, R. Djenadic, H. Hahn, Q. Zeng, Lattice distortion and stability of (Co0.2Cu0.2Mg0.2Ni0.2Zn0.2)O high-entropy oxide under high pressure, Mater. Today Adv. 8 (2020) 100102, https://doi.org/10.1016/j.mtadv.2020.100102.
[15] G.M. Tomboc, X. Zhang, S. Choi, D. Kim, L.Y.S. Lee, K. Lee, Stabilization, characterization, and electrochemical applications of high-entropy oxides: critical assessment of crystal phase-properties relationship, Adv. Funct. Mater. 32 (2022), https://doi.org/10.1002/adfm.202205142.
[16] T. Parida, A. Karati, K. Guruvidyathri, B.S. Murty, G. Markandeyulu, Novel rare-earth and transition metal-based entropy stabilized oxides with spinel structure, Scr. Mater. 178 (2020) 513–517, https://doi.org/10.1016/j.scriptamat.2019.12.027.
[17] M. Nasrollahzadeh, M. Sajjadi, S.M. Sajadi, Z. Issaabadi, Green Nanotechnology, first ed., Elsevier Ltd., 2019. https://doi.org/10.1016/B978-0-12-813586-0.00005-5.
[18] A. Amri, Z.T. Jiang, T. Pryor, C.Y. Yin, S. Djordjevic, Developments in the synthesis of flat plate solar selective absorber materials via sol-gel methods: a review, Renew. Sustain. Energy Rev. 36 (2014) 316–328, https://doi.org/10.1016/j.rser.2014.04.062.
[19] P.A.K. Nair, W.L. Vasconcelos, K. Paine, J. Calabria-Holley, A review on applications of sol-gel science in cement, Constr. Build. Mater. 291 (2021) 123065, https://doi.org/10.1016/j.conbuildmat.2021.123065.
[20] S. Ahmad, S. Munir, N. Zeb, A. Ullah, B. Khan, J. Ali, M. Bilal, M. Omer, M. Alamzeb, S.M. Salman, S. Ali, Green nanotechnology: a review on green synthesis of silver nanoparticles — an ecofriendly approach, Int. J. Ofnanomed. 14 (2019) 5087–5107, https://doi.org/10.2147/IJN.S200254.
[21] J.R.D. Santos, R.A. Raimundo, T.R. Silva, V.D. Silva, D.A. Macedo, F.J.A. Loureiro, M.A.M. Torres, D. Tonelli, U.U. Gomes, Nanoparticles of mixed-valence oxides MnXCO3-XO4 ($0 \leq X \leq 1$) obtained with agar-agar from red algae (rhodophyta) for oxygen evolution reaction, Nanomaterials 12 (18) (2022) 3170, https://doi.org/10.3390/nano12183170.
[22] J.R.D. Santos, F.J.A. Loureiro, J.P.F. Grilo, V.D. Silva, T.A. Simões, D.P. Fagg, D. A. Macedo, Understanding the cathodic polarisation behaviour of the misfit [Ca2CoO3−δ]q[CoO2] (C349) as oxygen electrode for IT-SOFC, Electrochim. Acta 285 (2018) 214–220, https://doi.org/10.1016/j.electacta.2018.08.018.
[23] J.V.A. Santos, M.A. Macedo, F. Cunha, J.M. Sasaki, J.G.S. Duque, BaFe12O19 thin film grown by an aqueous sol-gel process, Microelectronics J. 34 (2003) 565–567, https://doi.org/10.1016/S0026-2692(03)00049-1.
[24] J. Liu, Z. Xue, W. Zhang, M. Yan, Y. Xia, Preparation and properties of wet-spun agar fibers, Carbohydr. Polym. 181 (2018) 760–767, https://doi.org/10.1016/j.carbpol.2017.11.081.
[25] W.K. Lee, Y.Y. Lim, A.T.C. Leow, P. Namasivayam, J. Ong Abdullah, C.L. Ho, Biosynthesis of agar in red seaweeds: a review, Carbohydr. Polym. 164 (2017) 23–30, https://doi.org/10.1016/j.carbpol.2017.01.078.
[26] M. Fu, X. Ma, K. Zhao, X. Li, D. Su, High-entropy materials for energy-related applications, Iscience. 24 (3) (2021) 102177, https://doi.org/10.1016/j.isci.2021.102177.
[27] C. Sun, Y.J. Zhao, X.Y. Yuan, J.B. Li, H.B. Jin, Bimetal nanoparticles hybridized with carbon nanotube boosting bifunctional oxygen electrocatalytic performance, Rare Met. 41 (2022) 2616–2623, https://doi.org/10.1007/s12598-022-02021-1.

[28] J. Liu, C. Wang, L. Wang, Y. Zhao, J. Li, H. Jin, Microstructural control of Co3O4 nanoboxes for enhanced oxygen evolution in alkaline media, J. Alloys Compd. 835 (2020) 155290, https://doi.org/10.1016/j.jallcom.2020.155290.
[29] M.I. Jamesh, X. Sun, Recent progress on earth abundant electrocatalysts for oxygen evolution reaction (OER) in alkaline medium to achieve efficient water splitting – a review, J. Power Sources 400 (2018) 31–68, https://doi.org/10.1016/j.jpowsour.2018.07.125.
[30] P. Zhang, H. He, Rational rope-like CuCo2O4 nanosheets directly on Ni foam as multifunctional electrodes for supercapacitor and oxygen evolution reaction, J. Alloys Compd. 826 (2020) 153993, https://doi.org/10.1016/j.jallcom.2020.153993.
[31] Q. Wang, X. Liu, D. He, D. Wang, Fundamental comprehension, synthetic procedures and catalytic applications of high entropy oxide nanomaterials, Mater. Today 70 (2023) 218–236, https://doi.org/10.1016/j.mattod.2023.10.007.
[32] J.L. Braun, C.M. Rost, M. Lim, A. Giri, D.H. Olson, G.N. Kotsonis, G. Stan, D. W. Brenner, J.P. Maria, P.E. Hopkins, Charge-induced disorder controls the thermal conductivity of entropy-stabilized oxides, Adv. Mater. 30 (2018) 1–8, https://doi.org/10.1002/adma.201805004.
[33] C.C.L. McCrory, S. Jung, I.M. Ferrer, S.M. Chatman, J.C. Peters, T.F. Jaramillo, Benchmarking hydrogen evolving reaction and oxygen evolving reaction electrocatalysts for solar water splitting devices, J. Am. Chem. Soc. 137 (2015) 4347–4357, https://doi.org/10.1021/ja510442p.
[34] N.J. Usharani, R. Shringi, H. Sanghavi, S. Subramanian, S.S. Bhattacharya, Role of size, alio-/multi-valency and non-stoichiometry in the synthesis of phase-pure high entropy oxide (Co, Cu, Mg, Na, Ni, Zn)O, Dalt. Trans. 49 (2020) 7123–7132, https://doi.org/10.1039/d0dt00958j.
[35] V. Nallathambi, L.K. Bhaskar, D. Wang, A.A. Naberezhnov, S.V. Sumnikov, E. Ionescu, R. Kumar, Tuning the mechanical and thermal properties of (MgNiCoCuZn)O by intelligent control of cooling rates, J. Eur. Ceram. Soc. 43 (2023) 4517–4529, https://doi.org/10.1016/j.jeurceramsoc.2023.03.016.
[36] Y. Gao, Y. Liu, H. Yu, D. Zou, High-entropy oxides for catalysis: status and perspectives, Appl. Catal. A Gen. 631 (2022) 118478, https://doi.org/10.1016/j.apcata.2022.118478.
[37] J. Su, Z. Cao, Z. Jiang, G. Chen, Y. Zhu, L. Wang, G. Li, High entropy oxide nanofiber by electrospun method and its application for lithium battery anode material, Int. J. Appl. Ceram. Technol. 19 (2022) 2004–2015, https://doi.org/10.1111/ijac.14021.
[38] X. Liu, Y. Xing, K. Xu, H. Zhang, M. Gong, Q. Jia, S. Zhang, W. Lei, Kinetically accelerated lithium storage in high-entropy (LiMgCoNiCuZn)O enabled by oxygen vacancies, Small 18 (2022) 1–11, https://doi.org/10.1002/smll.202200524.
[39] N.J. Usharani, A. Bhandarkar, S. Subramanian, S.S. Bhattacharya, Antiferromagnetism in a nanocrystalline high entropy oxide (Co, Cu, Mg, Ni, Zn)O: magnetic constituents and surface anisotropy leading to lattice distortion, Acta Mater. 200 (2020) 526–536, https://doi.org/10.1016/j.actamat.2020.09.034.
[40] R.A. Raimundo, T.R. Silva, J.R.D. Santos, A.J.M. Araújo, J.F.G.A. Oliveira, M. A. Morales, M.M. Soares, D.A. Macedo, Nickel oxide nanocatalyst obtained by a combined sol-gel and hydrothermal method for oxygen evolution reaction, MRS Commun. 13 (2023) 276–282, https://doi.org/10.1557/s43579-023-00340-7.
[41] L.S. Ferreira, T.R. Silva, V.D. Silva, R.A. Raimundo, T.A. Simões, F.J.A. Loureiro, D. P. Fagg, M.A. Morales, D.A. Macedo, Spinel ferrite MFe2O4 (M = Ni, Co, or Cu) nanoparticles prepared by a proteic sol-gel route for oxygen evolution reaction, Adv. Powder Technol. 33 (2022) 103391, https://doi.org/10.1016/j.apt.2021.12.010.
[42] R.A. Raimundo, J.N. Silva, T.R. Silva, A.J.M. Araújo, J.F.G.A. Oliveira, L.C. De Lima, M.A. Morales, M.M. Soares, D.A. Macedo, Synthesis of Co3O4-CoO nanocomposite and electrochemical assessment for oxygen evolution reaction, Green Chem. 341 (2023) 1–4, https://doi.org/10.1016/j.matlet.2023.134196.
[43] M. Moulavi, K. Kanade, D. Amalnerkar, A. Fatehmulla, A.M. Aldhafiri, M. Aslam Manthrammel, Synergistic surface basicity enhancement effect for doping of transition metals in nanocrystalline MgO as catalysts towards one pot Wittig reaction, Arab. J. Chem. 14 (2021) 103134, https://doi.org/10.1016/j.arabjc.2021.103134.
[44] V.D. Silva, R.A. Raimundo, T.A. Simões, F.J.A. Loureiro, D.P. Fagg, M.A. Morales, D.A. Macedo, E.S. Medeiros, Nonwoven Ni–NiO/carbon fibers for electrochemical water oxidation, Int. J. Hydrogen Energy. 46 (2021) 3798–3810, https://doi.org/10.1016/j.ijhydene.2020.10.156.
[45] M.C. Biesinger, B.P. Payne, A.P. Grosvenor, L.W.M. Lau, A.R. Gerson, R.S.C. Smart, Resolving surface chemical states in XPS analysis of first row transition metals, oxides and hydroxides: Cr, Mn, Fe, Co and Ni, Appl. Surf. Sci. 257 (2011) 2717–2730, https://doi.org/10.1016/j.apsusc.2010.10.051.
[46] M. Swadźba-Kwaśny, L. Chancelier, S. Ng, H.G. Manyar, C. Hardacre, P. Nockemann, Facile in situ synthesis of nanofluids based on ionic liquids and copper oxide clusters and nanoparticles, Dalt. Trans. 41 (2012) 219–227, https://doi.org/10.1039/C1DT11578B.
[47] X. Wang, B. Zhang, W. Zhang, M. Yu, L. Cui, X. Cao, J. Liu, Super-light Cu@Ni nanowires/graphene oxide composites for significantly enhanced microwave absorption performance, Sci. Rep. 7 (2017) 1584, https://doi.org/10.1038/s41598-017-01529-2.
[48] R. Al-Gaashani, S. Radiman, A.R. Daud, N. Tabet, Y. Al-Douri, XPS and optical studies of different morphologies of ZnO nanostructures prepared by microwave methods, Ceram. Int. 39 (2013) 2283–2292, https://doi.org/10.1016/j.ceramint.2012.08.075.
[49] W. Tang, S. Wang, W. Xiao, S. Du, X. Lu, S. Hoang, J. Ding, P.X. Gao, Pre-surface leached cordierite honeycombs for MnxCo3-xO4 nano-sheet array integration with enhanced hydrocarbons combustion, Catal. Today. 320 (2019) 196–203, https://doi.org/10.1016/j.cattod.2017.10.045.
[50] K.R. Park, J.E. Jeon, K. Kim, N. Oh, Y.H. Ko, J. Lee, S.H. Lee, J.H. Ryu, H.S. Han, S. Mhin, Synthesis of rod-type Co2.4Mn0.6O4 via oxalate precipitation for water splitting catalysts, Appl. Surf. Sci. 510 (2020) 145390, https://doi.org/10.1016/j.apsusc.2020.145390.
[51] Y. Lao, X. Huang, W. Jiang, X. Mo, J. Huang, Y. Qin, Q. Mo, X. Hui, Z. Yang, L. Liu, Structure-activity relationship study of high entropy oxides catalysts for oxygen evolution reaction, Chem. Eng. J. 481 (2023) 148428, https://doi.org/10.1016/j.cej.2023.148428.
[52] A. Vazhayil, L. Vazhayal, J. Thomas, S. Ashok C, N. Thomas, A comprehensive review on the recent developments in transition metal-based electrocatalysts for oxygen evolution reaction, Appl. Surf. Sci. Adv. 6 (2021) 100184, https://doi.org/10.1016/j.apsadv.2021.100184.
[53] R.M. Obodo, N.M. Shinde, U.K. Chime, S. Ezugwu, A.C. Nwanya, I. Ahmad, M. Maaza, P.M. Ejikeme, F.I. Ezema, Recent advances in metal oxide/hydroxide on three-dimensional nickel foam substrate for high performance pseudocapacitive electrodes, Curr. Opin. Electrochem. 21 (2020) 242–249, https://doi.org/10.1016/j.coelec.2020.02.022.
[54] Y. Zhang, W. Dai, P. Zhang, T. Lu, Y. Pan, In-situ electrochemical tuning of (CoNiMnZnFe)3O3.2 high-entropy oxide for efficient oxygen evolution reactions, J. Alloys Compd. 868 (2021) 159064, https://doi.org/10.1016/j.jallcom.2021.159064.
[55] D. Wang, Z. Liu, S. Du, Y. Zhang, H. Li, Z. Xiao, W. Chen, R. Chen, Y. Wang, Y. Zou, S. Wang, Low-temperature synthesis of small-sized high-entropy oxides for water oxidation, J. Mater. Chem. A 7 (2019) 24211–24216, https://doi.org/10.1039/C9TA08740K.
[56] M. Einert, M. Mellin, N. Bahadorani, C. Dietz, S. Lauterbach, J.P. Hofmann, Mesoporous high-entropy oxide thin films: electrocatalytic water oxidation on high-surface-area spinel (Cr0.2Mn0.2Fe0.2Co0.2Ni0.2)3O4 electrodes, ACS Appl. Energy Mater. 5 (2022) 717–730, https://doi.org/10.1021/acsaem.1c03190.
[57] S. Zhao, H. Wu, R. Yin, X. Wang, H. Zhong, Q. Fu, W. Wan, T. Cheng, Y. Shi, G. Cai, C. Jiang, F. Ren, Preparation and electrocatalytic properties of (FeCrCoNiAl0.1)Ox high-entropy oxide and NiCo-(FeCrCoNiAl0.1)Ox heterojunction films, J. Alloys Compd. 868 (2021) 159108, https://doi.org/10.1016/j.jallcom.2021.159108.
[58] H. Jiang, H. Zhang, Q. Kang, H. Ma, Y. Tong, F. Gao, Q. Lu, Rapid solvent-evaporation strategy for three-dimensional cobalt-based complex hierarchical architectures as catalysts for water oxidation, Sci. Rep. 9 (2019) 1–8, https://doi.org/10.1038/s41598-019-51979-z.
[59] M.E.G. Lyons, M.P. Brandon, The significance of electrochemical impedance spectra recorded during active oxygen evolution for oxide covered Ni, Co and Fe electrodes in alkaline solution, J. Electroanal. Chem. 631 (2009) 62–70, https://doi.org/10.1016/j.jelechem.2009.03.019.
[60] L.A. da Silva, V.A. Alves, M.A.P. da Silva, S. Trasatti, J.F.C. Boodts, Oxygen evolution in acid solution on IrO2 + TiO2 ceramic films. a study by impedance, voltammetry and SEM, Electrochim. Acta 42 (1997) 271–281, https://doi.org/10.1016/0013-4686(96)00160-0.
[61] G. Li, P.-Y.-A. Chuang, Identifying the forefront of electrocatalytic oxygen evolution reaction: electronic double layer, Appl. Catal. B Environ. 239 (2018) 425–432, https://doi.org/10.1016/j.apcatb.2018.08.037.